

Mono Vector-Quark Production at the LHC

Haiying Cai^{1,*}

¹*Department of Physics, Peking University, Beijing 100871, China*

Abstract

Vector-like quark is a common feature in many new physics models. We study the vector-like quark production as an s -channel resonance at the Large Hadron Collider for the vector-like quarks mainly mixing with the top- and bottom-quark in the Standard Model. We emphasize that the leptonic angular distribution can be used to discriminate various vector-like quark models.

arXiv:1210.5200v3 [hep-ph] 8 Nov 2012

*Electronic address: hycal@pku.edu.cn

I. INTRODUCTION

Vector-like quark (vector-quark) exists in many models of new physics (NP) beyond the Standard Model (SM), e.g. extra dimensional models, Little Higgs models, dynamical models, etc. The vector-quark, denoted by \mathcal{Q} , could mix with the SM quarks through Yukawa interaction. In particular, the mixing of vector-quark with the third generation quarks in the SM is quite common in the Little Higgs models [1] and composite Higgs boson models [2]. Several possibilities for their electroweak quantum numbers are listed in Ref. [3] (see Table I). The phenomenology of the vector-quark production in hadron collisions has been studied either in the pair production [4] or in the association production with a SM quark [5, 6]. In the work we consider the mono vector-quark production as an s -channel resonance via strong magnetic q - g - \mathcal{Q} couplings at the Large Hadron Collider (LHC). Depending on whether the vector-quark would mix with SM chiral quarks, we can further focus on the decay channel that the vector-quark decays into a top-quark plus a jet, i.e. $\mathcal{Q} \rightarrow tg$ and other electroweak decay channels. The top-quark polarization can be measured through the charged lepton angular distribution from top-quark decay inside the top-quark's rest frame and the polarization is sensitive to the chirality of the g - t - \mathcal{Q} coupling. The $SU(2) \times U(1)_Y$ charged and neutral currents will be modified according to the quantum numbers of vector-quarks after adding Yukawa mixings, therefore the branch ratios for vector-quark decay to electroweak gauge bosons vary in several vector-quark models. Discovering the vector-quark signal and further measuring the top-quark polarization would help us to distinguish several new physics models.

The q - g - \mathcal{Q} coupling is forbidden by the Ward Identity at the tree level. The interaction could be induced by the new physics (NP) at high energy scale (Λ). Rather than working in a ultra-violet completion theory, we adapt the approach of effective field theory (EFT) in this study. The vector-quark might carry different quantum number under the electroweak symmetry of the SM ($SU(2)_L \times U(1)_Y$). It could be a weak isospin singlet, doublet or triplet. Below we list all the possible gauge invariant dimension-6 effective operators which describe

TABLE I: Electroweak quantum numbers for vector-quark multiplets, which could mix with the SM quarks through the Yukawa interaction.

$\mathcal{Q}^{(m)}$	\mathcal{U}_1	\mathcal{D}_1	\mathcal{D}_2	\mathcal{D}_X	\mathcal{D}_Y	\mathcal{T}_X	\mathcal{T}_Y
	U	D	$\begin{pmatrix} U \\ D \end{pmatrix}$	$\begin{pmatrix} X \\ U \end{pmatrix}$	$\begin{pmatrix} D \\ Y \end{pmatrix}$	$\begin{pmatrix} X \\ U \\ D \end{pmatrix}$	$\begin{pmatrix} U \\ D \\ Y \end{pmatrix}$
$SU(2)_L$	0	0	2	2	2	3	3
Y	2/3	-1/3	1/6	7/6	-5/6	2/3	-1/3

the strong magnetic g - q - \mathcal{Q} interaction:

$$\begin{aligned}
\mathcal{L}_{gq\mathcal{Q}} = & \frac{\kappa_{u,R}}{\Lambda^2} \bar{q}_L \sigma^{\mu\nu} \lambda^A \mathcal{S}_{u,R} \tilde{\phi} G_{\mu\nu}^A + \frac{\kappa_{d,R}}{\Lambda^2} \bar{q}_L \sigma^{\mu\nu} \lambda^A \mathcal{S}_{d,R} \phi G_{\mu\nu}^A \\
& + \frac{\kappa_{u,L}}{\Lambda^2} \bar{\mathcal{D}}_{2L} \sigma^{\mu\nu} \lambda^A u_R \tilde{\phi} G_{\mu\nu}^A + \frac{\kappa_{d,L}}{\Lambda^2} \bar{\mathcal{D}}_{2L} \sigma^{\mu\nu} \lambda^A d_R \phi G_{\mu\nu}^A \\
& + \frac{\kappa_{X,L}}{\Lambda^2} \bar{\mathcal{D}}_{XL} \sigma^{\mu\nu} \lambda^A u_R \phi G_{\mu\nu}^A + \frac{\kappa_{Y,L}}{\Lambda^2} \bar{\mathcal{D}}_{YL} \sigma^{\mu\nu} \lambda^A d_R \tilde{\phi} G_{\mu\nu}^A \\
& + \frac{\kappa_{X,R}}{\Lambda^2} \bar{\mathcal{T}}_{XR} \sigma^{\mu\nu} \lambda^A (\phi \tau^I q_L) G_{\mu\nu}^A + \frac{\kappa_{Y,R}}{\Lambda^2} \bar{\mathcal{T}}_{YR} \sigma^{\mu\nu} \lambda^A (\tilde{\phi} \tau^I q_L) G_{\mu\nu}^A, \quad (1)
\end{aligned}$$

where ϕ is the SM Higgs boson doublet, $G_{\mu\nu}^A$ is the field tensor of gluon and Λ is the cut off scale of our effective theory. Note that the τ^I denotes the weak isospin in the basis of $(+, 0, -)$. Table I shows the detailed gauge quantum number for all the vector-quarks scenarios.

The paper is organized as follows. In Sec. II we consider the simplest scenario where the vector-quark interacts with light quark only through the dimension-6 operators in the sense that it won't mix with the standard model chiral quarks. The top-quark is predominately left-handed polarized when it originates from a gauge singlet or triplet vector-quark. On the other hand, it is mainly right-handed polarized when it comes from a gauge doublet vector-quark decay. Since top-quark is the only "bare" quark in the SM, we consider the decay mode of $\mathcal{Q} \rightarrow t g$ to utilize the top-quark polarization to distinguish the gauge singlet/triplet and gauge doublet models. In the section III, we add the Yukawa interaction to couple the vector-quark to the SM chiral quarks such that fermions with the same quantum number can mix. Electroweak precision measurement i.e. the T parameter and $Z \rightarrow b\bar{b}$, are adopted to constrain the parameter space. After that, we proceed to analyze the channel of $pp \rightarrow \mathcal{Q} \rightarrow b l^+ \nu$. We derive the leptonic angular distribution with respect to the gluon moving

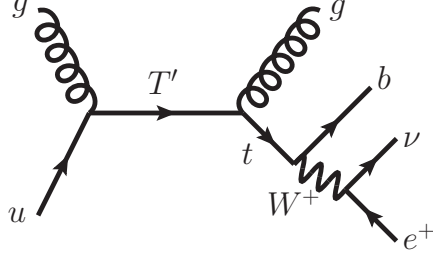


FIG. 1: Feynman diagram of the process of $ug \rightarrow \mathcal{Q} \rightarrow gt(\rightarrow be^+\nu_e)$.

direction in the center of mass frame of initial partons, which can be used to discriminate the singlet/triplet model from doublet model under certain assumptions. We are going to show that the mixing pattern for each vector quark scenario determines their discovery potentials in the LHC.

II. EXCITED QUARKS AND COLLIDER SIMULATION

We are interested in the following process that the mono produced vector-quark decays into a top-quark plus a jet (see Fig. 1 for Feynman diagram):

$$ug \rightarrow \mathcal{Q} \rightarrow tg, \quad t \rightarrow b\ell^+\nu, \quad (2)$$

with \mathcal{Q} carrying an electromagnetic charge $2/3$. In this section we assume that \mathcal{Q} does not mix with the chiral top quark in the SM such that they can only decay through dimension-6 operators. For clarity, we only include the positively charged state in the following discussion. Furthermore, the leptonic decay mode of the top-quark is considered in the analysis because the top-quark spin is maximally correlated with the charged lepton ℓ^+ . The drawback is the neutrino is invisible. It escapes the detection and yields a signature of large missing energy (\cancel{E}_T) at the collider. One has to determine the neutrino momentum to fully reconstruct the top-quark kinematics, which is the key for the top-quark polarization measurement.

After the spontaneously breaking of the electroweak symmetry, the effective operators described by Eq. [1] induces an effective chromo-magnetic-dipole coupling of g - u - \mathcal{Q} as follows:

$$L \supset \frac{v}{\sqrt{2}\Lambda^2} \bar{q}\sigma^{\mu\nu} (f_L P_L + f_R P_R) \mathcal{Q} G_{\mu\nu}(k) + h.c. \quad (3)$$

where $v = 246$ GeV denotes the vacuum expectation value for the Higgs field and P_L , P_R are the chiral projectors. We further assume that the heavy quark \mathcal{Q} interacts with all three

up-type quark in the SM (u, c, t) universally. As we can see from its original dimension-6 form, for each vector-quark scenario the interaction should be either left handed or right handed depending on their representations in the $SU(2)$ gauge group, i.e. f_L and f_R can not be present simultaneously. This property makes the dimension-6 operators distinct from the dimension-5 operators written down in the excited quark model [7]. Similar FCNC anomalous magnetic dimension-6 operators with the heavy quark \mathcal{Q} replaced by the top quark are adopted to study the single top production [8–10], whose coupling bounds are recently explored in the ATLAS experiments [11].

Since the excited heavy quark \mathcal{Q} has an electric charge $2/3$, we denote it as one heavy vector like T -quark in the following. The single T -quark production cross section at the LHC is :

$$\sigma(qg \rightarrow T) = \frac{1}{S} \int dx_1 dx_2 \{f_{q/P}(x_1)f_{g/P}(x_2) + (x_1 \leftrightarrow x_2)\} \delta(\hat{s} - m_T^2) \frac{\pi \hat{s} v^2}{6\Lambda^4} (f_L^2 + f_R^2), \quad (4)$$

where $f_{i/P}$ is the so-called parton distribution function (PDF) describing the possibility of finding a parton i inside a proton with a momentum fraction x_i . In the simplified model, the decay width is :

$$\Gamma(T \rightarrow qg) = \frac{v^2(f_L^2 + f_R^2) (m_T^2 - m_q^2)^3}{6\pi\Lambda^4 m_T^3}, \quad (5)$$

which clearly displays that the branching ratio of $T \rightarrow tg$ increases with m_T while the branch ratios of $T \rightarrow ug, cg$ decrease with m_T , and they all approach to $1/3$ in the large m_T limit. Since our effective operators contribute to the quark-gluon final states in the hadron collider, the upper limit of the dijet cross section put constraints on the couplings f_L and f_R [12, 13]. The cross section σ times the CMS acceptance factor A for $pp \rightarrow T \rightarrow ug, cg$ at a 7 TeV LHC is compared with the corresponding CMS upper limit for the quark-gluon final state as shown in Fig. 2. When we choose the cut-off Λ to be 1.2 TeV, the magnetic coupling strength need to satisfy the conditions of $f_L < 3.0$, $f_R = 0$ (or $f_L = 0$, $f_R < 3.0$). In this paper, we consider the relatively small magnetic coupling scenario. The inclusive cross section for the process of $qg \rightarrow T \rightarrow b\ell^+\nu g$ with $\ell^+ = e^+, \mu^+$ when the center of mass energy is 7 TeV, 8 TeV and 14 TeV is also plotted in Fig. 2. We choose the couplings to be $f_L = 0.5$, $f_R = 0$ (or $f_L = 0$, $f_R = 0.5$) with the cut-off Λ fixed to be 1.2 TeV.

The top-quark polarization can be best measured in its leptonic decay mode $t \rightarrow b\ell^+\nu$. The collider signature of interest to us is one charged lepton, two jets plus large missing

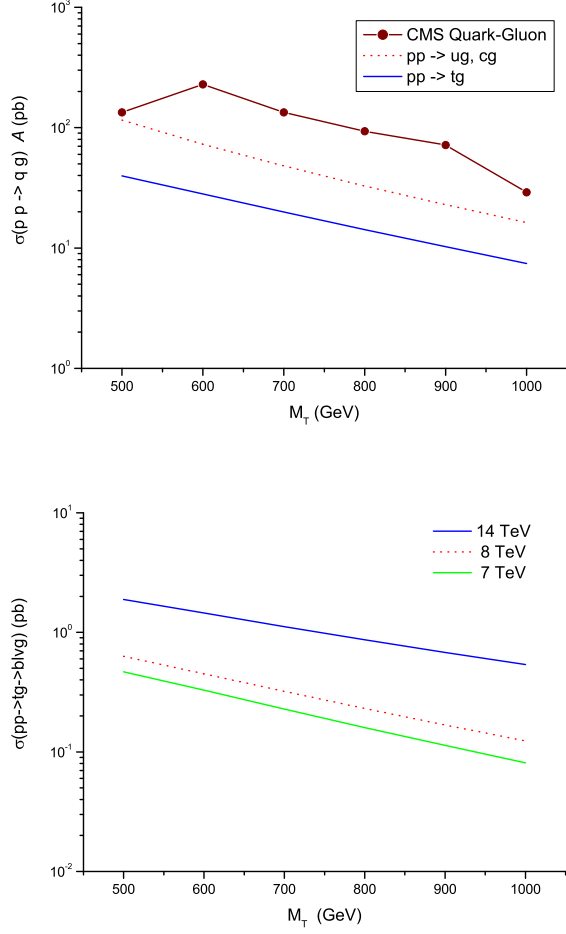


FIG. 2: The upper panel plot is the inclusive cross section (in the unit of picobarn) times CMS acceptance A for the process $pp \rightarrow T \rightarrow qq$ at a 7 TeV LHC. The red dotted line is for ug and cg final states via one excited T -quark, the blue solid line is for tg final state via one excited T -quark and the dark red line is the CMS upper limit for quark-gluon final states. The couplings are chosen as $f_L = 3.0$ and $f_R = 0$ while the cut-off scale Λ is fixed at 1.2 TeV. The lower panel plot is the inclusive cross section for the process $pp \rightarrow T \rightarrow qq$ at 7 TeV, 8 TeV and 14 TeV LHC in the green solid line, red dotted line and blue solid line respectively. The couplings are chosen as $f_L = 0.5$ and $f_R = 0$ with the same cut-off scale $\Lambda = 1.2$ TeV.

energy, where the large missing energy originates from the invisible neutrino and one of the two jets is the gluon in association with top-quark production and the other one is the b-quark from top-quark decay. The signature suffers from a few SM backgrounds as follows:

- Single- t production: single top-quark can be produced via the electroweak interaction in the Standard Model. It proceeds through the s -channel decay of a virtual W ($q\bar{q}' \rightarrow W^* \rightarrow t\bar{b}$), the t -channel exchange of a virtual W boson ($bq \rightarrow tq'$, $b\bar{q}' \rightarrow t\bar{q}$), and the associated production of a top-quark with two jets ($qq', gq \rightarrow tjj$). Note that tjj includes the process of $gb \rightarrow tW^-$ and with W^- subsequently decay into two jets. The single top plus one jet process is the intrinsic backgrounds as it yields exactly the same signature as the signal event. On the other hand, the top quark associated production with two jets process is the non-intrinsic background, since this process can only mimic the signal in the case that one of the two jets produced in association with the top-quark escapes the calorimeter detection.
- W + two jets production processes: among them are the Wbj production and the $Wb\bar{b}$ production which have the same signature as the signal events; the other one is Wjj production process but it requires one of the two jets to fake the b -jet. As to be shown later, it still contributes as the largest background even after including the small faking efficiency. Additional small background is from WZ production with Z gauge bosons decay into two jets.
- $t\bar{t}$ production: it is a non-intrinsic background because, in order to mimic the signal, either the two jets from the \bar{t} hadronic decay or the charged lepton from the \bar{t} leptonic decay need to get lost in the detector.

Both the signals and backgrounds are generated by MadGraph/MadEvent [14]. The CTEQ6L1 parton distribution functions [15] are used in this study. When generating the Wjj backgrounds, we impose soft cuts on the transverse momentum of the both jets, i.e. $p_T(j) > 5$ GeV, to avoid the collinear singularity. Note that such soft cuts do not affect our analysis as we impose much harder cuts on both jets in the following analysis. The inclusive cross section for the signal event i.e. $pp \rightarrow T \rightarrow tg$ with the following decays $t \rightarrow b\ell^+\nu$ ($\ell^+ = e^+, \mu^+$), is shown in the second column in Table II. For illustration we choose six benchmark masses for the T quark and choose $f_L = 0.5$ and $f_R = 0$. The cut off scale is set to be $\Lambda = 1.2$ TeV throughout this work. Other results of different couplings can be easily obtained by rescaling:

$$\sigma_s(f_L, f_R) = \sigma_s(f_L = 0.5, f_R = 0) 4 (f_L^2 + f_R^2). \quad (6)$$

TABLE II: Cross section (in the unit of fb) of the signal events for various m_T at the 14 TeV LHC (upper panel) and of the SM backgrounds (lower panel). The model parameters are chosen as $f_L = 0.5$, $f_R = 0$ and $\Lambda = 1.2$ TeV.

m_T (GeV)	no cuts	basic cuts	$P_T^g > 200$ GeV	$H_T > 400$ GeV	$\Delta M_W < 10$ GeV $\Delta M_t < 10$ GeV
500 GeV	1893.51	512.192	256.287	240.759	233.659
600 GeV	1453.86	417.329	322.756	304.365	295.569
700 GeV	1120.	335.439	292.542	277.59	268.687
800 GeV	869.751	276.362	255.054	242.617	235.703
900 GeV	680.2	223.344	211.95	200.387	194.299
1000 GeV	540.21	181.403	174.866	166.736	161.658

Backgrounds	no cuts	basic cuts	$P_t^g > 200$ GeV	$H_T > 400$ GeV	$\Delta M_W < 10$ GeV $\Delta M_t < 10$ GeV
Wjj	$1.8532 * 10^7$	13476.5	637.501	633.794	163.082
$Wb\bar{b}$	48054.	1191.74	13.215	12.014	3.604
Wbj	2774.2	36.758	0.277	0.277	0.139
WZ	544.13	99.494	0.449	0.422	0.027
tj	29619.	4214.78	311.0	294.71	281.38
tjj	28234.	5522.57	364.219	290.81	237.166
$t\bar{b}$	1025.1	247.649	12.945	12.004	9.718
$t\bar{b}j$	27745	975.237	40.230	31.907	26.358
$t\bar{t}(\bar{b}l\nu)$	25431.	118.254	3.178	1.272	0.0
total	$1.86954 * 10^7$	25883	1383.01	1277.21	721.474

To simulate a realistic detection, we impose the event-selection cuts as follows:

$$\begin{aligned}
p_T^b &> 20 \text{ GeV}, \quad |\eta_b| < 2.5, \\
p_T^\ell &> 20 \text{ GeV}, \quad |\eta_l| < 2.5, \\
\Delta R_{jj} &> 0.4, \quad \Delta R_{jl} > 0.4,
\end{aligned} \tag{7}$$

where $\Delta R(\equiv \sqrt{(\Delta\eta)^2 + (\Delta\phi)^2})$ is the separation between any two observable final state particles (not including neutrinos) , and $\Delta\phi$ and $\Delta\eta$ are the separation in azimuthal angle and rapidity, respectively. In order to let those non-intrinsic background to mimic the signals, additional veto cuts are demanded for jets or leptons which are not detected (either falling into a large rapidity region or carrying a too small transverse momentum to be detected),

$$\text{veto cuts : } p_T(j, \ell^\pm) < 10 \text{ GeV or } |\eta(j, \ell^\pm)| > 3.5 . \quad (8)$$

with η denoting the rapidity of the jets or leptons in the final state. The vetoing cut is imposed at the same time with the basic cut when we are performing the events selection and the corresponding cross section after the event selection is presented in the third column of Table II. We model the detector resolution effects by smearing the final state energy according to

$$\frac{\delta E}{E} = \frac{\mathcal{A}}{\sqrt{E/\text{GeV}}} \oplus \mathcal{B}, \quad (9)$$

where we take $\mathcal{A} = 10(50)\%$ and $\mathcal{B} = 0.7(3)\%$ for leptons (jets). In addition, we require that one jet is tagged as b -jet with a tagging efficiency is 50%. We also apply a mistagging rate for charm-quark $\epsilon_{c \rightarrow b} = 10\%$ for $p_T(c) > 50 \text{ GeV}$. The mistagging for a light jet is $\epsilon_{u,d,c,s,g \rightarrow b} = 0.67\%$ for $p_T(j) < 100 \text{ GeV}$ and 2% for $p_T(j) > 250 \text{ GeV}$. For $100 \text{ GeV} < p_T(j) < 250 \text{ GeV}$, we linearly interpolate the fake rate given above.

At this stage of the analysis, the background rate is one or two order of magnitude larger than the signal rate. Moreover, the dominate background comes from the Wjj process, followed by the single-top plus jets production and other small background processes. In order to study the efficient cuts that can significantly suppress the background rates while keeping most of the signal rates, we examine the p_T distributions of the leading- p_T jet as shown in Fig. 3. The leading jet in the signal originates from the light jet produced in association with the top-quark. Owing to the large m_T , the leading jet peaks in the large p_T region. On the contrary, the leading jets in the backgrounds, either from the QCD radiation or from the W -boson decay, tend to peak in the small p_T region. Such a distinct difference enables us to impose a hard cut on the first leading jet,

$$p_T(j_{1st}) > 200 \text{ GeV}, \quad (10)$$

to suppress the huge backgrounds. In the fourth column of Table II we show the cross sections after the above cuts. This cut increases the signal-to-background ratio by a factor

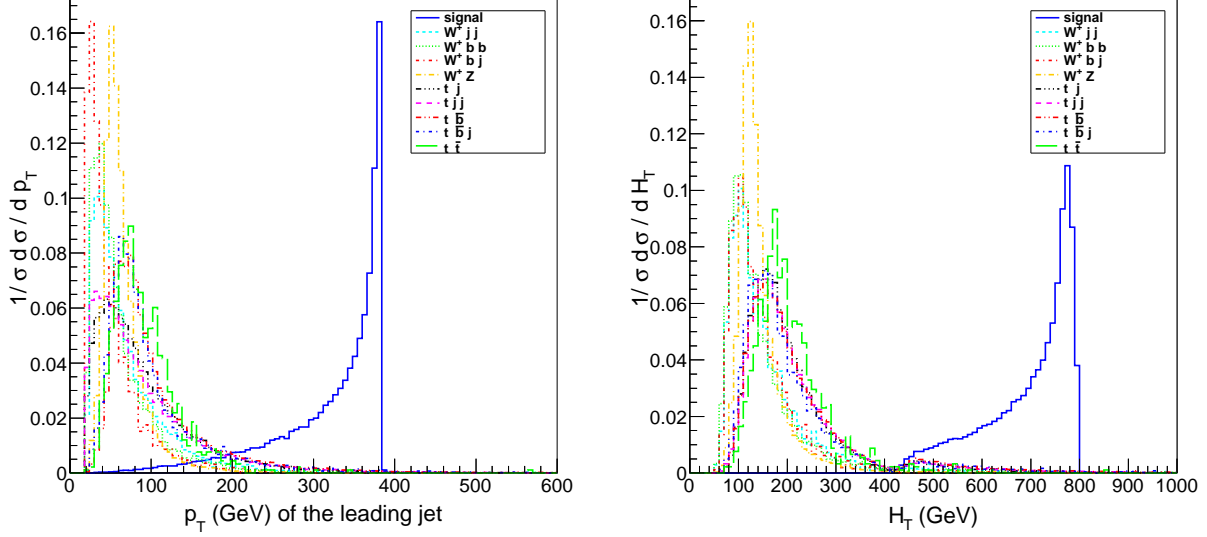


FIG. 3: The left panel is the p_T distribution of the leading jet in the signal and background events after the basic and veto selection cuts. The right panel is the H_T distribution of all the final objects in signal and background events after the basic and veto selection cuts. Each distribution plot is normalized.

of 17.2 while keeping about 92% of the signals for $m_T = 800\text{GeV}$. The biggest reduction in the background rate comes from the Wjj production, but all the other backgrounds are reduced sizably as well.

One can further impose a hard cut on the H_T variable, the scalar sum of the transverse momentum of all the measurable objects in the final states i.e. $H_T = \sum p_T^i + \cancel{E}_T$ with i sum over the visible objects. The H_T distribution of the signal events peaks in the large $H_T > 400\text{ GeV}$ region, while the one of the SM backgrounds is mostly located in the small $H_T < 400\text{ GeV}$ region (see Fig 3). But this cut does not influence both the signal and background too much after the hard $p_t(j_{1st}) > 200\text{ GeV}$ cut .

We are interested in measuring the top-quark polarization, which requires a full reconstruction of the top-quark kinematics. One confronts the invisible neutrino in the final state. Assuming the missing transverse momentum (\cancel{E}_T) comes entirely from the neutrino, i.e.

$$p_\nu(x) = -\cancel{E}_T(x), \quad p_\nu(y) = -\cancel{E}_T(y), \quad (11)$$

the longitudinal momentum of the neutrino can be reconstructed by the on-shell condition

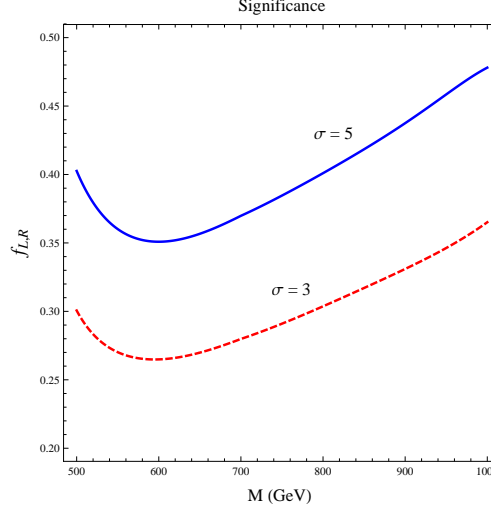


FIG. 4: Contour of the discovery potential of the signal at the 14 TeV LHC with an integrated luminosity of 1 fb^{-1} . Both the 3σ exclusion limit $S/\sqrt{S+B} = 3$, (red-dashed line) and the 5σ discovery limit $S/\sqrt{B} = 5$ (blue-solid line) are shown in the figure.

of W -boson:

$$m_W^2 = (p_\ell + p_\nu)^2. \quad (12)$$

The quadratic equation yields a two-fold solution. We only pick the real solutions and abandon the complex ones due to the W gauge boson's width effect. Since the W -boson comes from a top quark, both solutions are used to reconstruct the top quark mass, so that we can pick the one which gives a mass closer to 173 GeV. The neutrino momentum reconstruction is conducted after the large p_T cut. After neutrino reconstruction we are able to determine the kinematics of both the W -boson and top quark. Two mass-window cuts around m_W and m_t are imposed to optimize the signal events,

$$\Delta M_W = |m_{\ell\nu} - m_W| < 10 \text{ GeV}, \quad \Delta M_t = |m_{\ell\nu b} - m_t| < 10 \text{ GeV}. \quad (13)$$

Fig. 4 plots discovery potential of the signal event in the plane of m_T and f_L ($f_R = 0$) after the mass-window cuts. We display both the 5σ discovery limit and the 3σ exclusion limit in the significance plot, which shows that it is promising to observe the single T -quark production at the LHC with an integrated luminosity of 1 fb^{-1} .

The behavior of the angle between the lepton in the rest frame of the top quark and the top quark moving direction in the center of mass frame can be factorized out and described

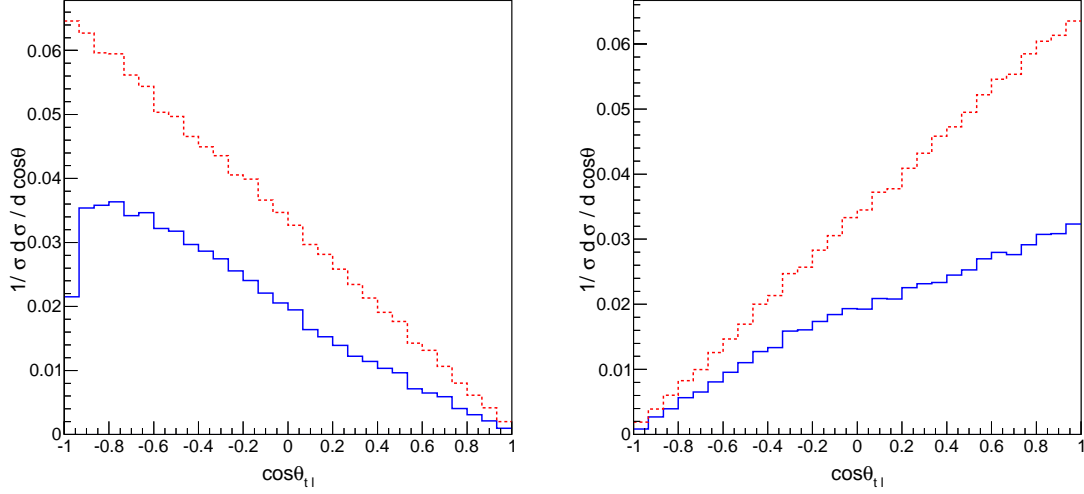


FIG. 5: The $\cos \theta$ distribution of the signal with no cut (dashed line) and after the mass-window cuts (solid line): (a) the singlet/triplet T -quark, (b) the doublet T -quark .

by the following equation [16, 17]:

$$\frac{1}{\sigma} \frac{d\sigma}{d \cos \theta_\ell} = \frac{1}{2} (1 + a \cos \theta_\ell), \quad (14)$$

where $a = 1$ for the pure left-handed heavy top quark and $a = -1$ for the pure right-handed heavy top quark. Figure 5 displays the $\cos \theta_\ell$ distribution with no cut and after imposing the mass-window cut.

III. VECTOR-QUARK AND SM QUARK MIXING

In the previous discussion we assume the vector-quarks do not mix with the SM quark at the tree level. However one could write down a gauge-invariant Yukawa interaction between the vector-quark and the SM quarks as follows:

$$\begin{aligned} \mathcal{L}_Y = & -y_u \bar{q}_L H^c u_R - y_d \bar{q}_L H d_R - \lambda_u \bar{q}_L H^c \mathcal{U}_R - \lambda_u \bar{\mathcal{D}}_{2L} H^c u_R - \lambda_d \bar{\mathcal{D}}_{2L} H d_R \\ & - \lambda_u \bar{\mathcal{D}}_{XL} H u_R - \lambda_u \bar{q}_L \tau^a H^c \mathcal{T}_{XR}^a - \lambda_u \bar{q}_L \tau^a H \mathcal{T}_{YR}^a - M \bar{\mathcal{U}}_L \mathcal{U}_R \\ & - M \bar{\mathcal{D}}_{2L} \mathcal{D}_{2R} - M \bar{\mathcal{D}}_{XL} \mathcal{D}_{XR} - M \bar{\mathcal{T}}_{XL} \mathcal{T}_{XR} - M \bar{\mathcal{T}}_{YL} \mathcal{T}_{YR}, \end{aligned} \quad (15)$$

The Yukawa interaction generates a mixing between the SM quarks and the vector-quarks at the tree level after the spontaneous symmetry-breaking. The singlet vector-quark and the

triplet vector-quark exhibit a similar mixing pattern, while the doublet vector-quark have a different mixing pattern. For simplicity, we consider the scenario that the vector-quarks mix only with the third-generation quark in the SM. Consider one pair of vector-quark $T'_{L,R}$ or one pair of vector-quark $B'_{L,R}$ which will mix with the chiral top-quark $t'_{L,R}$ or the chiral bottom quark $b'_{L,R}$ in the following way :

$$t'_{L,R} = \cos \theta_{L,R}^u t_{L,R} + \sin \theta_{L,R}^u T_{L,R}, \quad (16)$$

$$T'_{L,R} = -\sin \theta_{L,R}^u t_{L,R} + \cos \theta_{L,R}^u T_{L,R}, \quad (17)$$

$$b'_{L,R} = \cos \theta_{L,R}^d b_{L,R} + \sin \theta_{L,R}^d B_{L,R}, \quad (18)$$

$$B'_{L,R} = -\sin \theta_{L,R}^d b_{L,R} + \cos \theta_{L,R}^d B_{L,R}, \quad (19)$$

where $t_{L,R}$ and $T_{L,R}$ labels the physical top-quark and heavy vector-quark, respectively. Defining $x_t = \lambda_u v / \sqrt{2}$ and $x_b = \lambda_d v / \sqrt{2}$, the mixing angle can be calculated by diagonalizing the mass matrix. For the singlet/triplet vector-quark we obtain

$$\sin \theta_{u(d)}^L = \frac{M x_{t(b)}}{\sqrt{(M^2 - m_{t(b)}^2)^2 + M^2 x_{t(b)}^2}}, \quad (20)$$

$$\sin \theta_{u(d)}^R = \frac{m_{t(b)} x_{t(b)}}{\sqrt{(M^2 - m_{t(b)}^2)^2 + M^2 x_{t(b)}^2}}. \quad (21)$$

while for the doublet vector-quark

$$\sin \theta_{u(d)}^L = \frac{m_{t(b)} x_{t(b)}}{\sqrt{(M^2 - m_{t(b)}^2)^2 + M^2 x_{t(b)}^2}}, \quad (22)$$

$$\sin \theta_{u(d)}^R = \frac{M x_{t(b)}}{\sqrt{(M^2 - m_{t(b)}^2)^2 + M^2 x_{t(b)}^2}}. \quad (23)$$

Since the mixing would inevitably modify the W - t - b and Z - b - b couplings in the SM, the electroweak precision measurements at the low energy would severely constrain the mixing parameters [18]. Before proceeding with the further analysis, we are going to consider the low energy precision test in several vector-quark models and put bounds on the parameter space using current experimental constraints. When fixing x_b , the parameter describing the mixing of the bottom-quark and the vector-quark, the stringent constraint in the (M, x_t) parameter space of the singlet and doublet vector-quark models is from the T -parameter, while it is from the Z - b - b coupling for the triplet vector-quark model. The mixing of vector-quark with standard model chiral quark modifies the charged current of W_1^μ gauge bosons

and the neutral current of W_3^μ gauge bosons simultaneously and the mass splitting among the fermions will contribute to T parameter through the vacuum polarization of the gauge bosons [19, 20]. For the singlet vector-quark \mathcal{U}_1 , two types of doublet vector-quark \mathcal{D}_2 and \mathcal{D}_X and the triplet vector-quark \mathcal{T}_X , their specific contributions to T parameter are formulated in Eq. [24-27]:

$$\Delta T_{\mathcal{U}_1} = \frac{3}{16\pi s_W^2 c_W^2} [\sin^2 \theta_u^L \theta_+(y_T, y_b) - \sin^2 \theta_u^L \theta_+(y_t, y_b) - \cos^2 \theta_u^L \sin^2 \theta_u^L \theta_+(y_T, y_t)] \quad (24)$$

$$\begin{aligned} \Delta T_{\mathcal{D}_X} = & \frac{3}{16\pi s_W^2 c_W^2} [\sin^2 \theta_u^L \theta_+(y_T, y_b) - \sin^2 \theta_u^L \theta_+(y_t, y_b) \\ & + (\sin^2 \theta_u^L + \sin^2 \theta_u^R) \theta_+(y_t, y_X) + (\cos^2 \theta_u^L + \cos^2 \theta_u^R) \theta_+(y_T, y_X) \\ & + 2 \sin \theta_u^L \sin \theta_u^R \theta_-(y_t, y_X) + 2 \cos \theta_u^L \cos \theta_u^R \theta_-(y_T, y_X) \\ & - (4 \cos^2 \theta_u^L \sin^2 \theta_u^L + \cos^2 \theta_u^R \sin^2 \theta_u^R) \theta_+(y_t, y_T) \\ & - 4 \cos \theta_u^L \sin \theta_u^L \cos \theta_u^R \sin \theta_u^R \theta_-(y_t, y_T)] \end{aligned} \quad (25)$$

$$\begin{aligned} \Delta T_{\mathcal{D}_2} = & \frac{3}{16\pi s_W^2 c_W^2} [(\cos^2(\theta_u^L - \theta_d^L) + \sin^2 \theta_u^R \sin^2 \theta_d^R - 1) \theta_+(y_t, y_b) \\ & + (\cos^2(\theta_u^L - \theta_d^L) + \cos^2 \theta_u^R \cos^2 \theta_d^R) \theta_+(y_T, y_B) \\ & + (\sin^2(\theta_u^L - \theta_d^L) + \cos^2 \theta_d^R \sin^2 \theta_u^R) \theta_+(y_t, y_B) \\ & + (\sin^2(\theta_u^L - \theta_d^L) + \sin^2 \theta_d^R \cos^2 \theta_u^R) \theta_+(y_T, y_b) \\ & + 2 \cos(\theta_u^L - \theta_d^L) (\sin \theta_u^R \sin \theta_d^R \theta_-(y_t, y_b) + \cos \theta_u^R \cos \theta_d^R \theta_-(y_T, y_B)) \\ & + 2 \sin(\theta_u^L - \theta_d^L) (\cos \theta_d^R \sin \theta_u^R \theta_-(y_t, y_B) - \sin \theta_d^R \cos \theta_u^R \theta_-(y_T, y_b)) \\ & - \cos^2 \theta_u^R \sin^2 \theta_u^R \theta_+(y_t, y_T) - \cos^2 \theta_d^R \sin^2 \theta_d^R \theta_+(y_b, y_B)] \end{aligned} \quad (26)$$

$$\begin{aligned}
\Delta T_{\tau_x} = & \frac{3}{16\pi s_W^2 c_W^2} \left[((\cos \theta_d^L \cos \theta_u^L + \sqrt{2} \sin \theta_d^L \sin \theta_u^L)^2 + 2 \sin^2 \theta_d^R \sin^2 \theta_u^R - 1) \theta_+(y_t, y_b) \right. \\
& + 2\sqrt{2}(\cos \theta_d^L \cos \theta_u^L + \sqrt{2} \sin \theta_d^L \sin \theta_u^L) \sin \theta_d^R \sin \theta_u^R \theta_-(y_t, y_b) \\
& + ((\cos \theta_u^L \sin \theta_d^L - \sqrt{2} \cos \theta_d^L \sin \theta_u^L)^2 + 2 \cos^2 \theta_d^R \sin^2 \theta_u^R) \theta_+(y_t, y_B) \\
& - 2\sqrt{2}(\cos \theta_u^L \sin \theta_d^L - \sqrt{2} \cos \theta_d^L \sin \theta_u^L) \cos \theta_d^R \sin \theta_u^R \theta_-(y_t, y_B) \\
& + ((-\sqrt{2} \cos \theta_u^L \sin \theta_d^L + \cos \theta_d^L \sin \theta_u^L)^2 + 2 \cos^2 \theta_u^R \sin^2 \theta_d^R) \theta_+(y_T, y_b) \\
& - 2\sqrt{2}(-\sqrt{2} \cos \theta_u^L \sin \theta_d^L + \cos \theta_d^L \sin \theta_u^L) \cos \theta_u^R \sin \theta_d^R \theta_-(y_T, y_b) \\
& + ((\sin \theta_d^L \sin \theta_u^L + \sqrt{2} \cos \theta_d^L \cos \theta_u^L)^2 + 2 \cos^2 \theta_d^R \cos^2 \theta_u^R) \theta_+(y_T, y_B) \\
& + 2\sqrt{2}(\sin \theta_d^L \sin \theta_u^L + \sqrt{2} \cos \theta_d^L \cos \theta_u^L) \cos \theta_d^R \cos \theta_u^R \theta_-(y_T, y_B) \\
& + (2 \sin^2 \theta_u^L + 2 \sin^2 \theta_u^R) \theta_+(y_t, y_X) + 4 \sin \theta_u^L \sin \theta_u^R \theta_-(y_t, y_X) \\
& + (2 \cos^2 \theta_u^L + 2 \cos^2 \theta_u^R) \theta_+(y_T, y_X) + 4 \cos \theta_u^L \cos \theta_u^R \theta_-(y_T, y_X) \\
& - (\cos^2 \theta_d^L \sin^2 \theta_d^L + 4 \cos^2 \theta_d^R \sin^2 \theta_d^R) \theta_+(y_b, y_B) \\
& \left. - 4 \cos \theta_d^L \sin \theta_d^L \cos \theta_d^R \sin \theta_d^R \theta_-(y_b, y_B) - \cos \theta_u^L{}^2 \sin \theta_u^L{}^2 \theta_+(y_T, y_t) \right] \quad (27)
\end{aligned}$$

where $y_i = m_i^2/m_Z^2$ is the dimensionless fermion mass squared rescaled by the inverse mass squared of the Z gauge bosons. I have already checked that all the divergence are cancelled due to the unitary property of mixing matrix and the relation between those mass eigenstates. Since the T parameter measures the effect of custodial symmetry breaking, The functions $\theta_+(y_1, y_2)$ and $\theta_-(y_1, y_2)$ are zeroes when $y_1 = y_2$ and they are defined by the Ref. [20] :

$$\theta_+(y_1, y_2) = y_1 + y_2 - \frac{2y_1 y_2}{y_1 - y_2} \log \frac{y_1}{y_2} \quad (28)$$

$$\theta_-(y_1, y_2) = 2\sqrt{y_1 y_2} \left(\frac{y_1 + y_2}{y_1 - y_2} \log \frac{y_1}{y_2} - 2 \right) \quad (29)$$

Another source of T parameter contribution comes from the Higgs mass deviation from the its reference value $m_{href} = 120$ GeV:

$$\Delta T_h = -\frac{3}{16\pi c^2} \log \left(\frac{m_h^2}{m_{href}^2} \right) . \quad (30)$$

The electroweak precision measurement gives the fit for the T parameter is $T = 0.05 \pm 0.11$ [23]. Assuming the Higgs mass is 125 GeV [21, 22] , and adding two sources of T parameter contribution, the contour of T -parameter in (M, x_t) parameter space for the singlet vector-quark and doublet vector-quarks are plotted in Figure 6(a-d). For the singlet

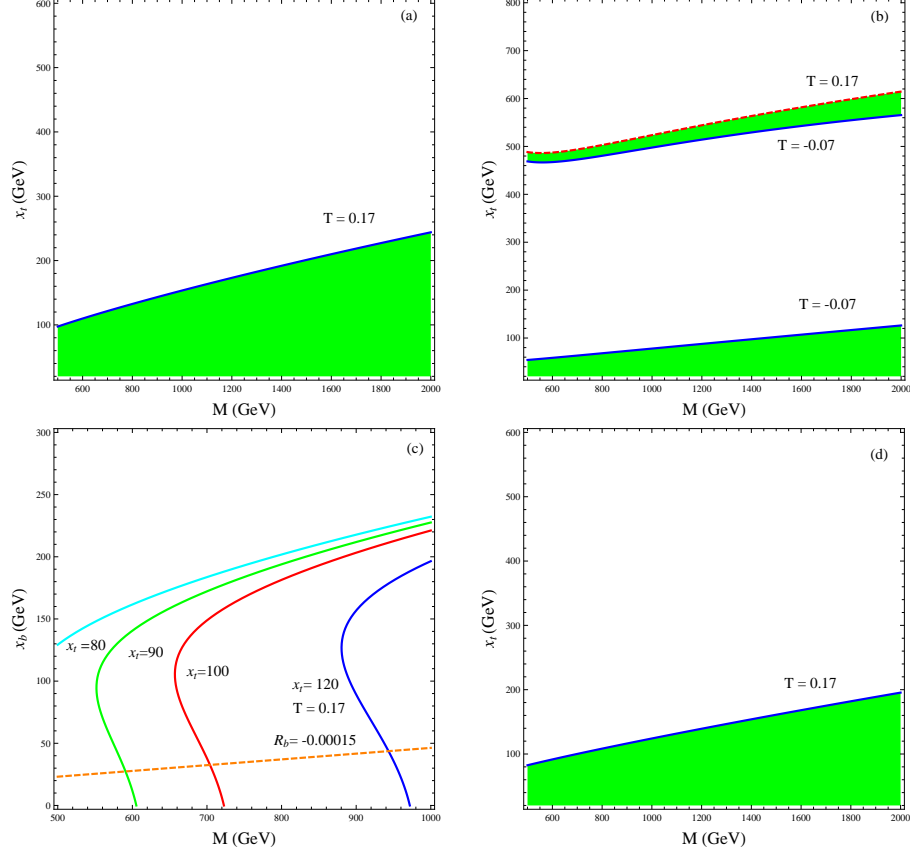


FIG. 6: (a) T parameter constraint for M and x_t in the singlet \mathcal{U}_1 model ; (b) T parameter constraint for M and x_t in the doublet \mathcal{D}_X model; (c) T parameter and R_b constraints for M and x_b in the doublet \mathcal{D}_2 model with x_t fixed to be 80, 90, 100, 120 GeV ; (d) T parameter constraint for M and x_t in the doublet \mathcal{D}_2 model with x_b fixed to be 20 GeV.

scenario as depicted by Fig. 6(a), only the Higgs gives a very small negative contribution and the singlet top quark can achieve larger positive contributions, therefore we get a positive T -parameter deviation in the interested vector-quark mass region. Requiring $T < 0.17$ and varying the gauge invariant mass M in the range of (500 – 1000) GeV, the upper limit for the top quark mixing parameter x_t should be in the range of (97.4 – 153.4) GeV. Since the mixing pattern and hyper charge assignment determine the $SU(2)$ gauge bosons currents, we see another situation in the \mathcal{D}_X doublet vector quark scenario. The Fig. 6(b) illustrates the T parameter constraint for the \mathcal{D}_X doublet model with the same mixing parameter x_t as the singlet model. The extra $5/3$ charged heavy quark X in the doublet model does not mix with any standard model quarks, but they will contribute to the $\Delta T_{\mathcal{D}_X}$. The heavy quark loop

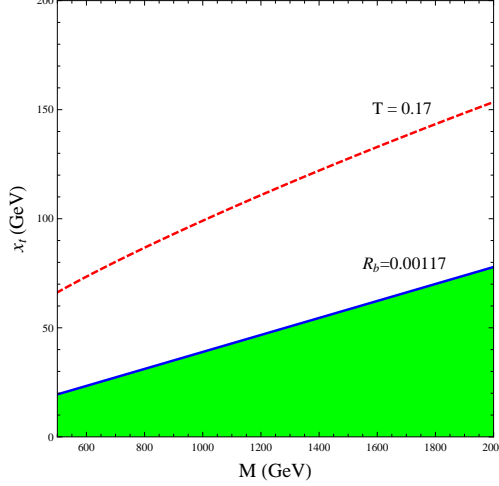


FIG. 7: T parameter and R_b constraints for M and x_t in the triplet \mathcal{T}_X vector-quark model .

effects can achieve notable positive T parameter deviation when x_t is large while they give notable negative T parameter deviation when the x_t is small. Requiring $-0.07 < \Delta T < 0.17$, two stringent green bands in the (M, x_t) plane are the permitted parameter space. We are more interested in the lower green band located in the small x_t region. As the gauge invariant mass varies in the range of $(500 - 1000)\text{GeV}$, the negative T parameter bound constrains the x_t to be in the range of $(54 - 78)\text{GeV}$. For the doublet model with one heavy top quark and one heavy bottom quark, there will be two independent mixing parameters x_t and x_b for the up type quark and down type quark respectively. The T parameter mainly constrains the x_t and the other mixing parameter x_b is constrained by the $z \rightarrow b\bar{b}$ which will be considered following. In the Fig. 6(c), the cyan curve, green curve, red curve and the blue curve depict the upper bound $T = 0.17$ in the (M, x_b) parameter space for four sample values $x_t = 80, 90, 100, 120 \text{ GeV}$. As we can see, in the low x_b region which is allowed by the R_b constraints, the T parameter is not sensitive to the x_b but sensitive to the other mixing parameter x_t and the upper bound for gauge invariant mass M will increase as we enhance the value of x_t . Fig. 6(d) plots the $\Delta T_{\mathcal{D}_2}$ dependence on M and x_t with the fixed value $x_b = 20 \text{ GeV}$. Similar to the singlet model the T parameter mainly receives positive contribution from the heavy fermions in the \mathcal{D}_2 doublet model. After imposing the upper bound of $T < 0.17$, we can find that x_t is constrained to be in the range of $(81 - 123) \text{ GeV}$ in correspondence with the M in the range of $(500 - 1000)\text{GeV}$. Finally, we discuss the situation in the \mathcal{T}_X triplet model. Only the heavy top quark and the heavy bottom quark

in the triplet model will mix with the SM chiral quarks and the two mixing parameters are related to each other by virtue of $x_b = \sqrt{2}x_t$. The T parameter dependence for M and x_t is plotted in Fig. 7, which shows that it almost does not put any constraint in the parameter space compared with the tight R_b requirement.

In the situation with one pair of heavy bottom quark present, we need to consider the constraints from the $Z \rightarrow b\bar{b}$. Both the corrections to Z - b_L - b_L couplings and the corrections to Z - b_R - b_R couplings in the doublet model as well as in the triplet model are induced through the Yukawa mixing between the vector bottom quarks and the chiral bottom quarks. The δg_L^{NP} and δg_R^{NP} can be translated to be the deviation δR_b by the following formula Eq. [31]:

$$\delta R_b = 2R_b(1 - R_b) \left(\frac{g_L}{g_L^2 + g_R^2} \delta g_L^{NP} + \frac{g_R}{g_L^2 + g_R^2} \delta g_R^{NP} \right) \quad (31)$$

$$g_L = \frac{g}{c_W} \left(-\frac{1}{2} + \frac{1}{3}s_W^2 \right) \quad g_R = \frac{1}{3} \frac{g}{c_W} s_W^2, \quad (32)$$

where g_L and g_R are Z gauge bosons couplings to the left handed bottom quark and the right handed bottom quark in the Standard Model. R_b is defined as $\Gamma(Z \rightarrow b\bar{b})/\Gamma(Z \rightarrow \text{hadrons})$ with its SM value $R_b = 0.21578_{-0.0008}^{+0.0005}$. The deviation δR_b due to the new physics effects is constrained by electroweak measurements to be [23] :

$$\delta R_b = 0.00051 \pm 0.00066 \quad (33)$$

We can write down the Z - b_L - b_L couplings and the Z - b_R - b_R couplings in the \mathcal{D}_2 doublet model and in the \mathcal{T}_X triplet model. For the doublet model we have:

$$g_{ZbL} = \frac{g}{c_W} \left(-\frac{1}{2} + \frac{1}{3}s_W^2 \right) = g_{ZbL}^{sm} \quad (34)$$

$$g_{ZbR} = -\frac{1}{2} \frac{g}{c_W} \sin^2 \theta_d^R + \frac{1}{3} \frac{g}{c_W} s_W^2 = -\frac{1}{2} \frac{g}{c_W} \sin^2 \theta_d^R + g_{ZbR}^{sm} \quad (35)$$

while for triplet model we have :

$$g_{ZbL} = -\frac{1}{2} \frac{g}{c_W} \sin^2 \theta_d^L + \frac{g}{c_W} \left(-\frac{1}{2} + \frac{1}{3}s_W^2 \right) = -\frac{1}{2} \frac{g}{c_W} \sin^2 \theta_d^L + g_{ZbL}^{sm} \quad (36)$$

$$g_{ZbR} = -\frac{g}{c_W} \sin^2 \theta_d^R + \frac{1}{3} \frac{g}{c_W} s_W^2 = -\frac{g}{c_W} \sin^2 \theta_d^R + g_{ZbR}^{sm} \quad (37)$$

Substituting Eq.[34- 37] into Eq.[31], we get the R_b deviation due to the vector-quarks in the doublet model and in the triplet model respectively, which in turn gives stringent constraints for x_b and x_t in each scenario. As we can see from Fig. 6(c) which depicts the

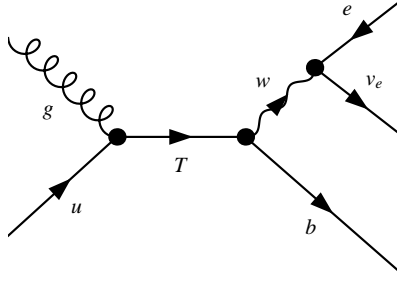


FIG. 8: Feynman diagram for single- T production and decay ($ug \rightarrow T \rightarrow bW^+ \rightarrow b\ell^+\nu_\ell$).

situation for the \mathcal{D}_2 doublet model, the negative R_b bound limits the x_b parameter to be in the range of $(23 - 46)$ GeV as M varies from 500 GeV to 1000 GeV. Fig. 7 shows that it is the upper limit of $R_b < 0.00117$ which put constraints on M and x_t for the \mathcal{T}_X triplet model. The green band is the allowed parameter space, i.e. for $500 \text{ GeV} < M < 1000 \text{ GeV}$, we need $20 \text{ GeV} < x_t < 39 \text{ GeV}$.

In this section we still consider the T -quark is produced via anomalous q - T - g couplings, but it could decay through the Yukawa interaction shown above. Note that after the mixing the T -quark as an s -channel resonance is no longer purely polarized. After adding the Yukawa mixing, the T -quark gets three additional decay modes opened: th , tZ and bW^+ . Here we proceed to analyze the process of $gq \rightarrow T \rightarrow bW^+$ with a subsequent W -boson leptonic decay (see Fig. 8 for Feynman diagrams), yielding a collider signature of $b\ell^+ \cancel{E}_T$. The main SM backgrounds are (1) W^+j where the light jet can mimic bottom quark; (2) W^+bj as well as t -channel single-top production $qb \rightarrow q't \rightarrow W^+bj$, in both cases we require that one of non- b tagged jets escapes detecting; (3) s -channel single-top production channel, $q\bar{q}' \rightarrow t\bar{b} \rightarrow W^+b\bar{b}$, where one of the bottom quarks escapes the detection. The basic cuts to trigger the events are:

$$\begin{aligned}
p_t^b &> 50 \text{ GeV}, & |\eta_b| &< 2.0, \\
p_t^l &> 20 \text{ GeV}, & |\eta_l| &< 2.4, \\
\Delta R_{bl} &> 0.7.
\end{aligned} \tag{38}$$

The cut table for the signal event (singlet case and doublet case) at the bench mark point

TABLE III: Cross section (fb) of the signal process $pp \rightarrow T \rightarrow bW^+ \rightarrow b\ell^+\nu$ and SM backgrounds for various kinematics cuts. The top table is for the singlet vector-quark with the choice of $f_L = 0$, $f_R = 0.2$ and $m_T = 800$ GeV. The middle table is for the doublet vector-quark with the choice of $f_L = 0.3$, $f_R = 0$ and $m_T = 800$ GeV and with an addition input $x_b = 20$ GeV. The bottom table is for the SM backgrounds.

x_t (GeV) no cuts basic cuts $P_t^b > 200$ GeV $\Delta R_{\nu\ell} < 1.5$ $\Delta m_W < 10\text{GeV}$					
40 GeV	211.8	73.643	69.841	66.283	66.283
60 GeV	223.1	77.059	73.121	69.596	69.596
80 GeV	228.02	80.046	76.056	72.237	72.237
100 GeV	230.44	80.216	76.518	73.199	73.199
120 GeV	232.18	81.890	77.595	74.019	74.019
x_t (GeV) no cuts basic cuts $P_t^b > 200$ GeV $\Delta R_{\nu\ell} < 1.5$ $\Delta m_W < 10\text{GeV}$					
40 GeV	166.25	57.847	54.921	52.336	52.336
60 GeV	114.36	39.694	38.088	36.115	36.115
80 GeV	88.792	30.314	28.968	27.552	27.552
100 GeV	75.728	25.369	24.426	23.211	23.211
120 GeV	68.41	22.599	21.70	20.732	20.732
SM bg no cuts basic cuts $P_t^b > 200$ GeV $\Delta R_{\nu\ell} < 1.5$ $\Delta m_W < 10\text{GeV}$					
w^+j	$1.95 * 10^7$	5889.06	175.97	175.97	175.97
w^+bj	2774.2	80.32	1.942	1.248	1.248
tj	29619	5386.22	42.947	7.405	7.405
$t\bar{b}$	1025.1	22.14	0.28	0.22	0.22
total	$1.95334 * 10^7$	11377.7	221.139	184.843	184.843

$m_T = 800$ GeV as well as for the background is shown in Table III. The third column shows the numbers of event after the basic cut. We demand b -tagged when imposing the basic cut where the veto cut for the non-intrinsic background events are also included. The b -tagging requirement effectively reduces the Wj background by a factor of 0.5×10^{-3} , while it still

keeps about 1/3 signal events. In the signal event the b -jet comes from the heavy vector-

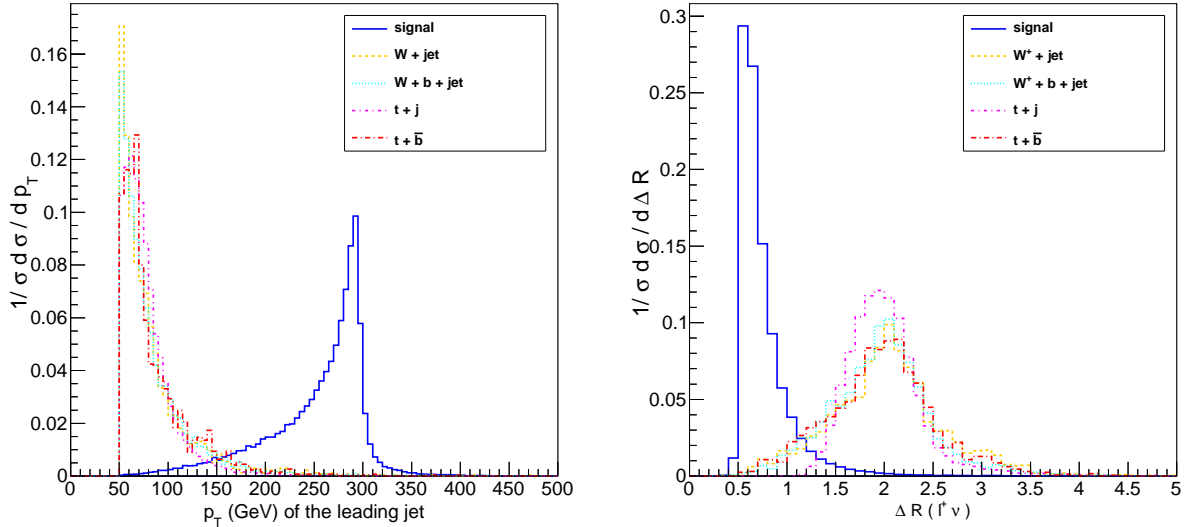


FIG. 9: (a) The p_T distribution of the leading jet after the basic and veto selection cut ; (b) the distribution of the $\Delta R(\ell^+\nu)$ between the lepton and the reconstructed neutrino after the basic and veto selection cut. Each distribution is normalized.

quark decay. It carries a large p_T . On the contrary, the b -jets in the background events, either from the gluon splitting or from the top-quark decay, exhibit a relatively soft p_T . The difference can be seen from Fig. 9(a) where the p_T distribution of the b -jet is plotted. Following the basic cut and b -tagging, we impose a hard p_T cut on the b -jet,

$$p_T(b) > 200 \text{ GeV}. \quad (39)$$

As shown in Table III the cut reduces the background more than one order of magnitude, but it leaves the signal events almost untouched. The reason that we do not consider the non-intrinsic background events from $W^+b\bar{b}$ and W^+Z is that $b\bar{b}$ from either gluon splitting or Z bosons decay can not simultaneously pass the veto cut as well as the hard $p_T(b)$ cut .

To fully reconstruct the signal event, the kinematics of the invisible neutrino is to be determined from the W -boson on-shell condition. We pick up the solution with a smaller magnitude in the two-fold solutions. The W -bosons from the heavy vector-quark T decay is highly boosted such that its decay products, the lepton and neutrino, tend to collimate and yield a small $\Delta R(\ell^+, \nu)$ separation as we can see from the blue-solid curve in Fig 9(b).

On the other hand, the background events are more evenly distributed in the relative large $\Delta R(\ell^+, \nu)$ region.

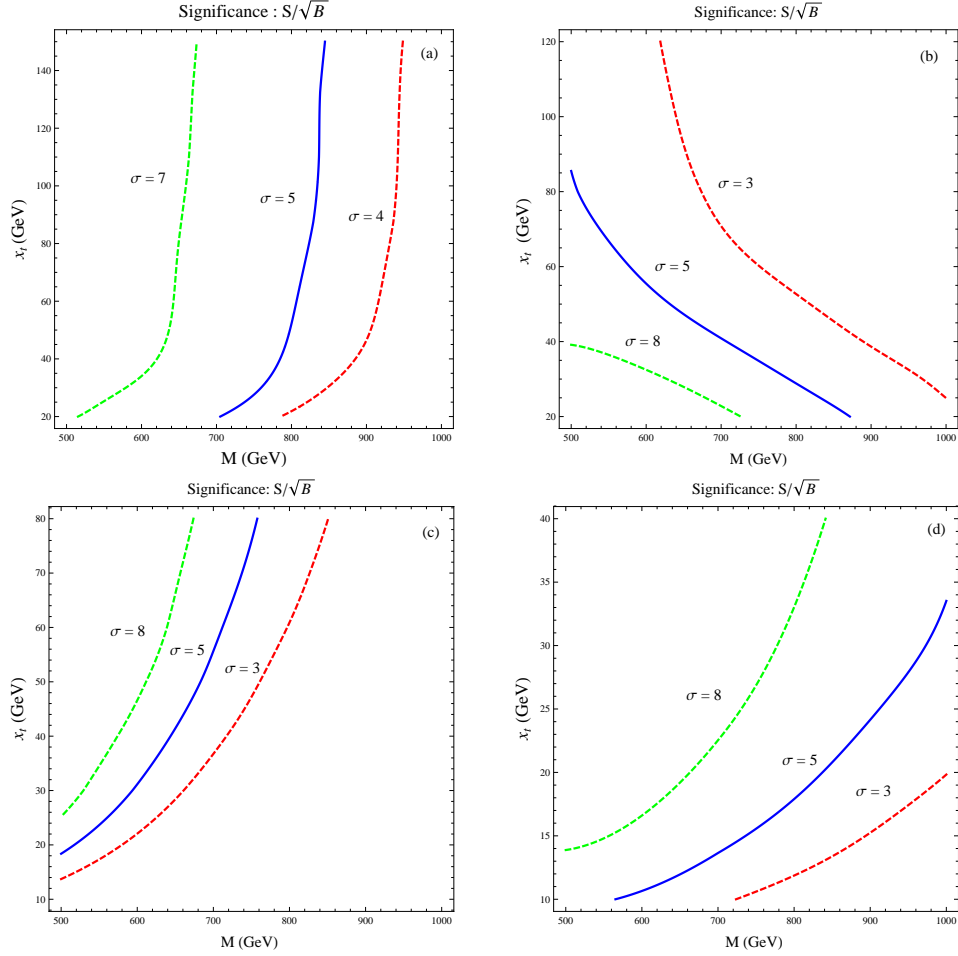


FIG. 10: Significance contour in the (x, M) parameter space: (a) the singlet \mathcal{U}_1 model ($f_R = 0.2$); (b) the doublet \mathcal{D}_2 model ($f_L = 0.3$ and $x_b = 20$ GeV); (c) the doublet \mathcal{D}_X model ($f_L = 0.6$) ; (d) the triplet \mathcal{T}_X model ($f_R = 0.3$).

Fig. 10 displays the significance contours at the 14 TeV LHC for several vector-quark models. The doublet \mathcal{D}_Y is ignored since there is no heavy T -quark in that model, and the triplet \mathcal{T}_Y models is not considered either because it has a very small branching ratio for the decay of $T \rightarrow W^+b$. We will emphasize some characteristic in those contours and illustrate the reasons as follows. The \mathcal{U}_1 , \mathcal{D}_X and \mathcal{T}_X models exhibit a similar pattern of the discovery potential, i.e. x_t increases with M for a fixed significance. While the doublet \mathcal{D}_2 model shows a different pattern as x_t decreases with M . The difference is caused by

the decay branching ratio of the vector-quark in various models [18]. The branching ratio of $T \rightarrow W^+b$ decay always increases as the value of x_t is enhanced in the \mathcal{U}_1 , \mathcal{D}_X and \mathcal{T}_X models. However in the \mathcal{D}_2 model the corresponding branching ratio can be approximated by $x_b^2/(x_b^2 + 2x_t^2)$ in the large M limit. There is a tension exists between x_b and x_t and the branching ratio of $T \rightarrow W^+b$ decreases with x_t for a fixed x_b value, which leads to the slopping pattern displayed in Fig. 10(b). As we can see from the significance plot for the \mathcal{U}_1 singlet model with $f_R = 0.2$, that the significance contour is not sensitive to the mixing parameter in the large x_t region, such that the $\sigma = 5$ discovery limit curve clearly cuts the M to be less than 800 GeV . Note that the \mathcal{D}_X doublet model has a smaller discovery potential as indicated by its magnetic coupling. The reason is that the branching ratio of $T \rightarrow W^+b$ is suppressed by a factor of m_t^2/M^2 in that model as compared with the other three ones.

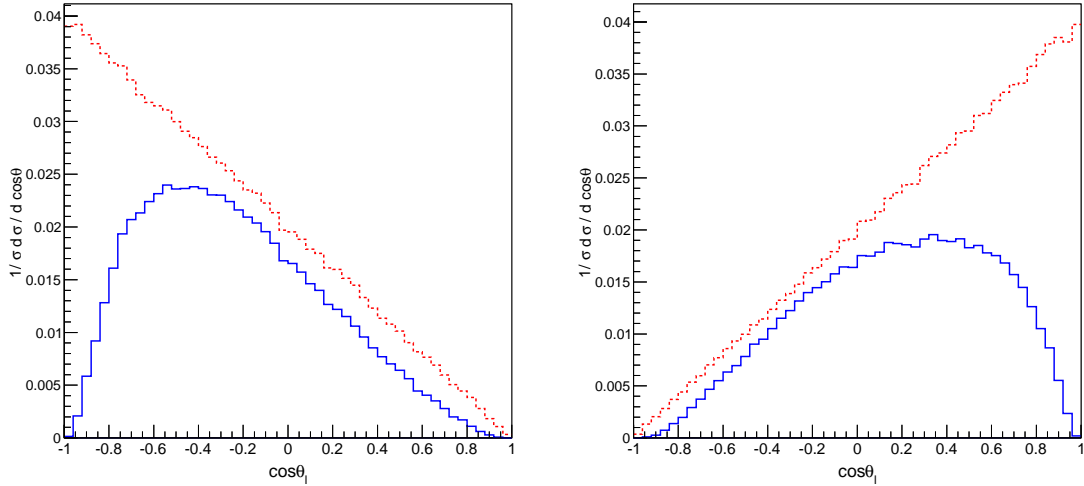


FIG. 11: The $\cos \theta_\ell$ distribution between the lepton and gluon moving directions with no cut (dashed line) and after the mass-window cut (solid line): (a) the singlet T -quark, (b) the doublet T -quark (when there is no heavy bottom quark or its effect can be ignored).

It is convenient to analyze the charged-lepton angular distribution between the lepton and the gluon moving directions in the center of mass frame, which can be used to distinguish the chiral property of T - b - W couplings. The differential cross sections with respect to $\cos \theta_\ell$

for the $ug \rightarrow b\ell^+\nu$ in vector-quark models in the limit of $m_W \ll \sqrt{s}$ are found to be:

$$\begin{aligned} \frac{1}{\hat{\sigma}} \frac{d\hat{\sigma}(u_R g \rightarrow b\ell^+\nu)}{d\cos\theta_\ell} &= \frac{g_W^{L\,2}}{g_W^{L\,2} + g_W^{R\,2}}(1 - \cos\theta_\ell) + \frac{g_W^{R\,2}}{g_W^{L\,2} + g_W^{R\,2}}(1 + \cos\theta_\ell) \\ &\quad - \frac{g_W^{R\,2}}{g_W^{L\,2} + g_W^{R\,2}} \cdot \mathcal{O}(m_W^2/s) \cdot \cos\theta_\ell \end{aligned} \quad (40)$$

$$\begin{aligned} \frac{1}{\hat{\sigma}} \frac{d\hat{\sigma}(u_L g \rightarrow b\ell^+\nu)}{d\cos\theta_\ell} &= \frac{g_W^{L\,2}}{g_W^{L\,2} + g_W^{R\,2}}(1 + \cos\theta_\ell) + \frac{g_W^{R\,2}}{g_W^{L\,2} + g_W^{R\,2}}(1 - \cos\theta_\ell) \\ &\quad + \frac{g_W^{R\,2}}{g_W^{L\,2} + g_W^{R\,2}} \cdot \mathcal{O}(m_W^2/s) \cdot \cos\theta_\ell \end{aligned} \quad (41)$$

Note that the $\mathcal{O}(m_W^2/s)$ correction is only for the term proportional to the right-handed T - b - W coupling. The detail derivation of exact results for the leptonic angular distribution in the rest frame of the heavy top quark is put in the Appendix. Fig. 11 displays the $\cos\theta_\ell$ distribution with no cut and after the mass-window cut. For the singlet \mathcal{U}_1 model, since the anomalous u - g - T interaction is right handed and the coupling of T - b - W is purely left handed, the angular distribution of $\cos\theta_\ell$ should be proportional to $(1 - \cos\theta)/2$ as indicated by Eq. [40] ; On the other hand, the anomalous u - g - T interaction is left handed and the coupling of T - b - W is also purely left handed in the doublet \mathcal{D}_X model, therefore the lepton angular distribution should be proportional to $(1 + \cos\theta)/2$, which is in coincidence with the analytic result (see Eq. [41]). The situation is more complicated in the doublet \mathcal{D}_2 model. In that model we have $g_W^L/g_W^R \approx (x_t m_t)/(x_b M)$ such that the angular distribution shows the superposition of $(1 \mp \cos\theta)/2$. When $x_b \gg x_t$, the coupling of T - b - W is mainly right-handed and the angular distribution is similar to the singlet \mathcal{U}_1 . In the other limit of $x_t \gg x_b$, the decay of $T \rightarrow bW^+$ is possible to be dominated by the left-handed coupling as long as M is not too large, so that its angular distribution is similar to the doublet \mathcal{D}_X . The leptonic angular distribution should serve as an effective analyzing power when the $V - A$ chiral structure of the T - b - W vertex is not too much modified.

IV. CONCLUSION

In this paper, the single heavy top quark production via strong magnetic interaction is studied and we explore the possibility for vector-quarks to be discovered in both the anomalous decay and electroweak decay channel. The leptonic angular distribution is a favored analyzing power for identifying the top quark polarization and distinguish varieties

of vector-quark models. We use the collider simulation to explain that the top polarization in the channel of $T \rightarrow tg$ is determined by the chirality property of the excited quarks. The Yukawa mixing does not change the situation since the mixing only dilutes the corresponding branch ratio in each specific model. However the $V - A$ chiral structure of T - b - W is possible to be modified by those Yukawa mixing . We conduct a detail analysis for the parameter space constrained by the electroweak precision test in various vector-quark models. The channel of $T \rightarrow bW^+$ has very less standard model backgrounds, and the leptonic angular distribution in that channel can at least be utilized to distinguish the \mathcal{U}_1 singlet model from the \mathcal{D}_X doublet model. Once we found the signals of heavy T vector-quark and measured its chirality, we are capable to reconstruct its mass as a resonance in a single production process. Although we have shown that the LHC is sensitive to the signals of vector like quarks in the single production channel, the cross section of such process depends on the coupling strength of strong magnetic interactions, otherwise the pair production of heavy top quarks should be a better discovery channel .

Acknowledgments

I thank Qing-Hong Cao and Jian Wang for collaboration in the early stage. The work is supported in part by the postdoc foundation under the Grant No. 2012M510001.

Appendix A: Leptonic angular distribution in c.m. frame

We derive the moving direction of charged lepton relative to the gluon moving direction in the center of mass rest frame for the process $ug \rightarrow T \rightarrow b\ell^+\nu$. The \hat{z} axis is defined by the moving direction of the charged lepton ℓ^+ in the c.m. frame of the initial partons. Since the production and the decaying can be factorized using the narrow width approximation, we further have the mass on shell relation i.e. $k_W^2 = M_W^2$, such that the energy and momentum of the bottom quark is determined by energy-momentum conservation to be: $E_W = \frac{\sqrt{s}}{2}(1 + \frac{m_W^2}{s})$ and $p = \frac{\sqrt{s}}{2}(1 - \frac{m_W^2}{s})$. The four momentum for the initial partons and the bottom quark, the lepton and the intermediate W^+ gauge bosons can be expressed as:

$$p_g = (\frac{\sqrt{s}}{2}, -\frac{\sqrt{s}}{2} \sin \theta_\ell, 0, \frac{\sqrt{s}}{2} \cos \theta_\ell) \quad (\text{A1})$$

$$p_u = (\frac{\sqrt{s}}{2}, \frac{\sqrt{s}}{2} \sin \theta_\ell, 0, -\frac{\sqrt{s}}{2} \cos \theta_\ell) \quad (\text{A2})$$

$$k_b = (p, p \sin \theta_{b\ell} \cos \phi_{b\ell}, p \sin \theta_{b\ell} \sin \phi_{b\ell}, p \cos \theta_{b\ell}) \quad (\text{A3})$$

$$k_W = (E_W, -p \sin \theta_{b\ell} \cos \phi_{b\ell}, -p \sin \theta_{b\ell} \sin \phi_{b\ell}, -p \cos \theta_{b\ell}) \quad (\text{A4})$$

$$k_\ell = (E_\ell, 0, 0, E_\ell) \quad (\text{A5})$$

where θ_ℓ is polar angle for the incoming gluon makes with the lepton moving direction (\hat{z} -axis), $\theta_{b\ell}$ is angle between the bottom quark and the lepton and the $\phi_{b\ell}$ is the corresponding azimuthal angle. In the left-handed and right-handed strong magnetic interaction cases, the amplitude squared is calculated to be:

$$|M(u_L g \rightarrow b e^+ \nu)|^2 = \frac{64}{\Lambda^4} g_2^2 v^2 f_L^2 p_g \cdot p_u (g_W^L{}^2 s k_e \cdot p_u k_{\nu e} \cdot k_b + g_W^R{}^2 M_T^2 k_{\nu e} \cdot p_g k_e \cdot k_b) \cdot \frac{\pi \delta(k_W^2 - m_W^2)}{\Gamma_W m_W} \frac{C_F \cdot N_c}{((s - M_T^2)^2 + \Gamma_T^2 M_T^2)} \quad (\text{A6})$$

$$|M(u_R g \rightarrow b e^+ \nu)|^2 = \frac{64}{\Lambda^4} g_2^2 v^2 f_R^2 p_g \cdot p_u (g_W^L{}^2 M_T^2 k_e \cdot p_g k_{\nu e} \cdot k_b + g_W^R{}^2 s k_{\nu e} \cdot p_u k_e \cdot k_b) \cdot \frac{\pi \delta(k_W^2 - m_W^2)}{\Gamma_W m_W} \frac{C_F \cdot N_c}{((s - M_T^2)^2 + \Gamma_T^2 M_T^2)} \quad (\text{A7})$$

where $C_F = 4/3$ and $N_c = 3$ are the color factors. A symmetry exists between the f_L and f_R scenarios that $k_{\nu e}$ is exchanged with k_e and the (V-A) coupling g_W^L is exchanged with the (V+A) coupling g_W^R . Phrasing the final states phase space in the rest frame of the heavy top quark, the differential cross section is expressed as:

$$d\hat{\sigma} = \frac{1}{2s} \frac{|M|^2}{4 \cdot 3 \cdot 8} \frac{4}{(4\pi)^5} dE_b dE_\ell d \cos \theta_\ell d\phi_\ell d\phi_{b\ell} \quad (\text{A8})$$

with the following integration limits:

$$\begin{aligned} \frac{\sqrt{s}}{2} - E_b &< E_\ell < \frac{\sqrt{s}}{2} \\ 0 &< E_b < \frac{\sqrt{s}}{2}, \\ -1 &< \cos \theta_\ell < 1, \quad 0 < \phi_\ell, \phi_{b\ell} < 2\pi \end{aligned} \quad (\text{A9})$$

We have used the narrow width approximation for the W^+ gauge bosons when we are calculating the amplitude squared and the delta function can be written as :

$$\delta(k_W^2 - m_W^2) = \frac{1}{2\sqrt{s}} \delta \left(E_b - \frac{\sqrt{s}}{2} \left(1 - \frac{m_W^2}{s} \right) \right). \quad (\text{A10})$$

The $\cos \theta_{b\ell}$ is not independent which can be written in terms of E_b and E_ℓ by the following expression:

$$\cos \theta_{b\ell} = \frac{s - 2\sqrt{s}(E_b + E_\ell)}{2E_b E_\ell} + 1 \quad (\text{A11})$$

Now we put all the elements into the amplitude squared and after integrating out E_b , E_ℓ and two azimuthal angles of ϕ_ℓ and $\phi_{b\ell}$ we get the following differential cross sections with respect to $\cos \theta_\ell$ which depict the angular distribution of the charged lepton in the center of mass rest frame:

$$\begin{aligned} \frac{d\hat{\sigma}(u_L g \rightarrow b \ell^+ \nu)}{d \cos \theta_\ell} &= \frac{g_2^2 v^2 f_L^2}{3^2 2^{11} \pi^2 \Lambda^4} \frac{1}{\Gamma_W m_W} \frac{1}{s} \left(g_W^L{}^2 \cdot s (m_W^2 - s)^2 (2m_W^2 + s) \cdot (1 + \cos \theta_\ell) \right. \\ &\quad \left. - g_W^R{}^2 M_T^2 \left((m_W^2 - s)^2 (2m_W^2 + s) + 12m_W^4 s - 12m_W^2 s^2 + 12m_W^4 s \log \left[\frac{s}{m_W^2} \right] \right) \cos \theta_\ell \right. \\ &\quad \left. + g_W^R{}^2 M_T^2 (m_W^2 - s)^2 (2m_W^2 + s) \right) \cdot \frac{1}{((s - M_T^2)^2 + \Gamma_T^2)} \end{aligned} \quad (\text{A12})$$

$$\begin{aligned} \frac{d\hat{\sigma}(u_R g \rightarrow b \ell^+ \nu)}{d \cos \theta_\ell} &= \frac{g_2^2 v^2 f_R^2}{3^2 2^{11} \pi^2 \Lambda^4} \frac{1}{\Gamma_W m_W} \frac{1}{s} \left(g_W^L{}^2 \cdot M_T^2 (m_W^2 - s)^2 (2m_W^2 + s) \cdot (1 - \cos \theta_\ell) \right. \\ &\quad \left. + g_W^R{}^2 s \left((m_W^2 - s)^2 (2m_W^2 + s) + 12m_W^4 s - 12m_W^2 s^2 + 12m_W^4 s \log \left[\frac{s}{m_W^2} \right] \right) \cos \theta_\ell \right. \\ &\quad \left. + g_W^R{}^2 s (m_W^2 - s)^2 (2m_W^2 + s) \right) \cdot \frac{1}{((s - M_T^2)^2 + \Gamma_T^2)} \end{aligned} \quad (\text{A13})$$

As we can see, only the term proportional to the (V-A) coupling has exactly the $1 \pm \cos \theta_\ell$ distribution and the term proportional to the (V+A) coupling is slightly corrected to be $(1 \mp \cos \theta_\ell) \pm \mathcal{O}(m_W^2/s) \cos \theta_\ell$, the deviation can be ignored in the limit of $m_W \ll \sqrt{s}$.

-
- [1] N. Arkani-Hamed, A. G. Cohen, E. Katz, A. E. Nelson, T. Gregoire and J. G. Wacker, JHEP **0208**, 021 (2002) [hep-ph/0206020]; N. Arkani-Hamed, A. G. Cohen, E. Katz and A. E. Nelson, JHEP **0207**, 034 (2002) [hep-ph/0206021]; M. Schmaltz and D. Tucker-Smith, Ann. Rev. Nucl. Part. Sci. **55**, 229 (2005) [hep-ph/0502182].
 - [2] K. Agashe, R. Contino and A. Pomarol, Nucl. Phys. B **719**, 165 (2005) [hep-ph/0412089]; C. Anastasiou, E. Furlan and J. Santiago, Phys. Rev. D **79**, 075003 (2009) arXiv:0901.2117 [hep-ph]; G. Panico and A. Wulzer, JHEP **1109**, 135 (2011) arXiv:1106.2719 [hep-ph]; S. De Curtis, M. Redi and A. Tesi, JHEP **1204**, 042 (2012) arXiv:1110.1613 [hep-ph] .
 - [3] F. del Aguila, M. Perez-Victoria and J. Santiago, “Observable contributions of new exotic quarks to quark mixing,” JHEP **0009**, 011 (2000) [arXiv:hep-ph/0007316].
 - [4] R. Contino and G. Servant, JHEP **0806**, 026 (2008) arXiv:0801.1679 [hep-ph].
 - [5] R. Barcelo, A. Carmona, M. Chala, M. Masip and J. Santiago, Nucl. Phys. B **857**, 172 (2012) arXiv:1110.5914 [hep-ph].
 - [6] A. Atre, G. Azuelos, M. Carena, T. Han, E. Ozcan, J. Santiago and G. Unel, JHEP **1108**, 080 (2011) arXiv:1102.1987 [hep-ph].
 - [7] U. Baur, I. Hinchliffe and D. Zeppenfeld, Int. J. Mod. Phys. A **2**, 1285 (1987); U. Baur, M. Spira and P. M. Zerwas, Phys. Rev. D **42**, 815 (1990).
 - [8] E. Malkawi and T. M. P. Tait, Phys. Rev. D **54**, 5758 (1996) [hep-ph/9511337].
 - [9] M. Hosch, K. Whisnant and B. L. Young, Phys. Rev. D **56**, 5725 (1997) [hep-ph/9703450].
 - [10] J. A. Aguilar-Saavedra, Nucl. Phys. B **812**, 181 (2009) arXiv:0811.3842 [hep-ph].
 - [11] G. Aad *et al.* [ATLAS Collaboration], Phys. Lett. B **712**, 351 (2012) arXiv:1203.0529 .
 - [12] T. Han, I. Lewis and Z. Liu, JHEP **1012**, 085 (2010) arXiv:1010.4309 [hep-ph].
 - [13] CMS Collaboration, arXiv:1010.0203 [hep-ex].
 - [14] J. Alwall, P. Demin, S. de Visscher, R. Frederix, M. Herquet, F. Maltoni, T. Plehn and D. L. Rainwater *et al.*, JHEP **0709**, 028 (2007) arXiv:0706.2334 [hep-ph] ; J. Alwall, M. Herquet, F. Maltoni, O. Mattelaer and T. Stelzer, JHEP **1106**, 128 (2011)
 - [15] J. Pumplin, D. R. Stump, J. Huston, H. L. Lai, P. M. Nadolsky and W. K. Tung, JHEP **0207**, 012 (2002) [hep-ph/0201195].
 - [16] M. Jezabek and J. Kuhn, Nucl. Phys. B **320** (1989) 20.

- [17] G. Mahlon and S. J. Parke, Phys. Rev. D **53**, 4886 (1996) [hep-ph/9512264].
- [18] G. Cacciapaglia, A. Deandrea, D. Harada and Y. Okada, “Bounds and Decays of New Heavy Vector-like Top Partners,” JHEP **1011**, 159 (2010) arXiv:1007.2933 [hep-ph].
- [19] M. E. Peskin and T. Takeuchi, Phys. Rev. Lett. **65**, 964 (1990); Phys. Rev. D **46**, 381 (1992);
- [20] L. Lavoura and J. P. Silva, ”The Oblique corrections from vector - like singlet and doublet quarks” , Phys. Rev. D **47** (1993) 2046.
- [21] ATLAS Collaboration, ATLAS-CONF-2011-163. CERN Higgs Search Update Seminar, Status of Standard Model Higgs Search in ATLAS, July 4, 2012.
- [22] CMS Collaboration, CMS-PAS-HIG-11-032, CERN Higgs Search Update Seminar, Status of the CMS SM Higgs Search, July 4, 2012.
- [23] M. Baak, M. Goebel, J. Haller, A. Hoecker, D. Ludwig, K. Moenig, M. Schott and J. Stelzer, arXiv:1107.0975 [hep-ph].